



Polyvinyl alcohol-stabilized granular iron(III)-copper(II) binary oxide: an efficient adsorbent for phosphate removal from water

Jun Fu^a, Faming He^b, Gaosheng Zhang^{c,*}, Guodong Yuan^d

^aSino-Japan Friendship Center for Environmental Protection, No. 1 Yuhuan Road, Beijing 100029, P.R. China, email: fujunceec@gmail.com

^bShandong Yanhai Construction Resources Co. Ltd., No. 3-8 Kaifeng Road, Yantai, 264006, Shandong, P.R. China, email: hfm765@126.com

^cInstitute of Environmental Research at Greater Bay, Guangzhou University, 230 Waihuanxi Road, Guangzhou Higher Education Mega Center, Guangzhou 510006, P.R. China, Fax: +86 020 39366505; emails: zgs77@126.com, gszhang@yic.ac.cn (G. Zhang)

^dSchool of Environmental and Chemical Engineering, Zhaoqing University, Zhaoqing Road, Zhaoqing, 526061, Guangdong, P.R. China, email: Yuanguodong@zqu.edu.cn

Received 24 May 2018; Accepted 9 December 2018

ABSTRACT

Though powdered iron(III)-copper(II) binary oxide offers a good capacity for phosphate adsorption, it is unsuitable for direct use in fixed-bed systems, due to pore clogging and high pressure drop. To solve this problem, a novel granular iron(III)-copper(II) binary oxide sorbent (GFC) was successfully prepared using extrusion granulation method. The as-prepared GFC is cylindrical, with a diameter of ca. 2.0 mm and a length of 2.0–3.0 mm. Its adsorption for phosphate increased with temperature, decreased with an increase in pH value, but not significantly influenced by co-existing SO_4^{2-} , HCO_3^- , and SiO_3^{2-} , indicating its high selectivity for phosphate. Its maximal phosphorus (P) adsorption capacity is 20.2 mg/g at pH 5.5 ± 0.1 , superior to most of the granular sorbents reported in literature. For column tests, about 1,780 bed volumes of simulated phosphate-containing wastewater were treated before the phosphorus (P) concentration in the effluent reached the limit of 50 $\mu\text{g/L}$ recommended by the United States Environmental Protection Agency (USEPA). Therefore, GFC has a high potential for use in wastewater treatment to remove phosphate.

Keywords: Granular Fe-Cu binary oxide; Phosphate; Adsorption; Column test

1. Introduction

Phosphorus is an essential nutrient for life, but excessive phosphorus may contribute to eutrophication of water bodies, deteriorating water quality and posing a threat to aquatic organisms and human health. Phosphorus is often found in municipal and some industrial wastewaters. Its concentration in a typical raw municipal wastewater is approximately 10 mg/L with ortho-phosphate as the principal form [1–3]. To prevent eutrophication problem, the United States Environmental Protection Agency (USEPA)

has recommended 50 $\mu\text{g/L}$ as the maximum phosphorus level in water [4], and Florida Everglades Forever Act has recommended a more stringent mandate of 10 $\mu\text{g/L}$ of phosphorus in water [5,6]. Therefore, the wastewaters containing phosphorus must be treated to meet phosphorus limit, prior to being discharged to the receiving water bodies.

The main techniques employed for phosphate removal include chemical precipitation [7], ion exchange [6], adsorption [1], membrane treatment [8], biological processes [9], and constructed wetlands [10]. Chemical precipitation and biological processes are generally unable to satisfy the

* Corresponding author.

stringent effluent standards. Ion exchange, reverse osmosis, and membrane have the disadvantage of high capital cost. In contrast, adsorption is recognized as a cost-effective and reliable method, with the advantages of easy operation, low sludge production, and high efficiency at low phosphate concentrations [11]. Therefore, a variety of adsorbents have been developed and evaluated for phosphate removal, including metal oxides [12,13], layered double hydroxides [1,2], volcanic tephra [14], and biochar [15,16]. Among them, metal oxides have been extensively investigated because of their high affinity for phosphate. Moreover, composite adsorbents containing two (or more) metal oxides for phosphate removal has gained much attention because they inherit the advantages of parent materials and exhibit synergetic effect. Al-Fe hydr(oxides) [17], Ce-Zr binary nanoadsorbent [18], Fe-Mn binary oxide [19], Fe-Zr binary oxide [20], Fe-Al-Mn trimetal oxide [21], and Fe-La binary (hydro) oxide [22] have been synthesized and tested for phosphate removal.

Recently, a novel nanostructured iron(III)-copper(II) binary oxide adsorbent has been developed for effective phosphate removal over a wide pH range [23]. Moreover, the spent Fe-Cu binary oxide could be easily regenerated and reused, which makes the adsorbent a potentially attractive choice for the removal of phosphate from water. However, the obtained Fe-Cu binary oxide is powdered. Its inherited problems of pore clogging, high pressure drop, and mass loss during operations make it unsuitable for direct use in packed beds [24,25]. By far, the greatest use of powdered adsorbents occurs in slurry reactors and not in fixed beds. However, fixed-bed reactors are the more widely preferred type of reactors for large-scale applications. We were, therefore, motivated to turn powdered Fe-Cu binary oxide into granular one for practical applications. To this end, granules were first produced by extruding the mixture of powdered Fe-Cu binary oxide and liquid polyvinyl alcohol (PVA) as binder, in a similar way of making granular catalysts, pharmaceuticals and fertilizers [26,27]. Then, the granular Fe-Cu binary oxide was systematically evaluated for its phosphate removal potential under various operational conditions, including initial phosphorus concentration, pH, temperature, reaction time, and competing anions. Finally, it was investigated in column tests to assess its performance for phosphorus removal.

2. Materials and methods

2.1. Reagents

Chemicals used in this work were purchased from Sinopharm Chemical Reagent Beijing Co. (Beijing, China), including anhydrous potassium dihydrogen orthophosphate (KH_2PO_4) of guaranteed grade and other reagents of analytical grade. Phosphorus (P) stock solution was prepared by dissolving KH_2PO_4 in water, and phosphorus working solutions were freshly prepared by diluting the stock solution with deionized water. The concentrations of phosphate species were given as phosphorus element concentration in this study.

2.2. Preparation of granular Fe-Cu binary oxide adsorbent

Granular Fe-Cu binary oxide was prepared via a two-step process: (1) synthesis of Fe-Cu binary oxide

powder. The powder was prepared following the procedure of Li et al. [23]. Specifically, 270.3 g of ferric chloride hexahydrate ($\text{FeCl}_3 \cdot 6\text{H}_2\text{O}$) and 125 g of copper (II) sulfate pentahydrate ($\text{CuSO}_4 \cdot 5\text{H}_2\text{O}$) were dissolved in 15 L deionized water. Under vigorous agitation, sodium hydroxide solution (5 M NaOH) was added dropwise until the suspension pH was raised to 7.0. The solution was continuously stirred for 0.5 h, aged for 4 h at room temperature, and then washed several times with deionized water. The final suspension was filtered, dried at 55°C for 24 h, ground into powder, and stored in a desiccator for further use; and (2) granulation using polyvinyl alcohol as binder. Briefly, 40 g of polyvinyl alcohol (PVA 1799) was dissolved in 500 mL hot water (95°C, water bath) to yield a homogenous solution. Then the solution was cooled down to the room temperature. Hereafter, about 400 g powdered adsorbent was added into the solution and mixed adequately (about 1 h), making the mass ratio of binder and powder to be 1:10. The mixture was transferred to an extrusion machine to prepare noodle-like adsorbent with a diameter of about 2 mm. The obtained granules were then dried at 55°C and broken up manually into particles with a length of 2.0–3.0 mm.

2.3. GFC characterization

GFC was observed by a field scanning electron microscope (FE-SEM) (Hitachi S-4800, Japan) and analyzed by energy dispersive X-ray spectroscopy. To some extent, the surface area value of adsorbents could reflect their active surfaces for adsorbates. The specific surface area of GFC was measured via nitrogen adsorption using Brunauer–Emmett–Teller (BET) method with a Micromeritics ASAP 2020 surface area analyzer (Micromeritics Co., USA). X-ray diffraction (XRD) analysis was carried out on a D/Max-3A diffractometer (Rigaku Co., Japan) using Ni-filtered copper $\text{K}\alpha$ 1 radiation. FTIR spectra were collected on a Nicolet IS10 FTIR spectrophotometer (Thermo Scientific, USA) using a transmission model. Samples for FTIR analysis were prepared via grinding 1 mg of GFC with 80 mg of spectral grade KBr in an agate mortar and then pressed into pellets. The point of zero charge (pzc) of GFC was determined according to the slightly modified method described by Kinniburgh et al. [28]. Briefly, about 0.1 g GFC was added to bottles with 50 mL 0.01 M NaNO_3 and the mixture was stirred for 24 h, after which the rate of change in pH was very slow. Then the mixture was adjusted to various pH values with NaOH or HNO_3 solution. After agitation for 60 min for equilibrium, the initial pH was measured; then 1.5 g of NaNO_3 was added to each bottle to bring final electrolyte concentration to about 0.45 M. After additional 3 h, the final pH was measured. The results were plotted as ΔpH (final pH – initial pH) against final pH to determine pzc as the pH at which $\Delta\text{pH} = 0$.

2.4. Batch adsorption tests

Adsorption kinetics of phosphate was assessed at pH 7.0 ± 0.1 . About 1.0 g GFC was added into a 1.5 L glass vessel containing 1,000 mL 5.2 mg/L phosphorus solution. The mixture was then stirred with a magnetic stirrer at 180 rpm and $25^\circ\text{C} \pm 1^\circ\text{C}$. The solution pH was maintained at 7.0 ± 0.1 throughout the experiment by adding 0.1 M HNO_3 and/or NaOH. Approximately 5 mL aliquots were taken from the

mixture at certain time intervals, and then filtered through a 0.45 μm membrane filter for phosphorus analysis. In order to eliminate the effect of membrane adsorption, the first 3 mL of filtrate was deliberately discarded for all samples. The result indicated that adsorption reached equilibrium within 36 h. Thus, this equilibrium time was used in batch experiments.

The influence of solution pH on phosphate sorption was assessed via batch experiments. Briefly, 50 mg of GFC were added into 100-mL polyethylene bottles with 50 mL of 5 mg/L phosphorus solution. Solution pH was adjusted every 4 h with 0.01 M HNO_3 or/and NaOH solution to designated values in the range of 4.0–11.0 during the 36 h experiment. At the end, equilibrium pH was measured and the supernatant was filtered through a 0.45 μm membrane for phosphorus analysis.

Adsorption isotherm experiments were carried out by varying initial phosphorus concentrations (2.5–35 mg/L) at two pHs of 7.0 ± 0.1 and 5.5 ± 0.1 , respectively, with a total solution volume of 50 mL in 100-mL polyethylene bottles. The dose of GFC was fixed at 1 g/L. The bottles were shaken on an orbit shaker at 180 rpm for 36 h at $25^\circ\text{C} \pm 1^\circ\text{C}$ (298 K). The pH of mixtures was maintained by manually adjusting with 0.1 M NaOH and HNO_3 . At the end, all samples were filtered by a 0.45 μm membrane filter and analyzed for phosphorus. In addition, batch experiments were also conducted at 15 ± 1 (288 ± 1) and $35^\circ\text{C} \pm 1^\circ\text{C}$ (308 ± 1 K), respectively, to investigate the effect of temperature on phosphate adsorption.

The influences of coexisting anions (SO_4^{2-} , HCO_3^- , and SiO_3^{2-}) on phosphate removal were also evaluated using fixed initial phosphorus concentration of 5.0 mg/L, fixed GFC dose of 1.0 g/L, fixed solution pH at 7.0 ± 0.1 , and varied concentration of coexisting substances (0.1 to 10 mM). After stirring at 180 rpm and $25^\circ\text{C} \pm 1^\circ\text{C}$ for 36 h, the solution was filtered by a 0.45 μm membrane filter for phosphorus analysis.

2.5. Column tests

Fixed-bed column tests were performed using perspex columns with an inner diameter of 1.9 cm and a total length of 32 cm. Approximately 32 g of GFC was packed into the column, making a packed height of 25.0 cm and a volume of 70.8 mL. A simulated wastewater containing 3.2 mg/L phosphorus was used as feeding solution. The pH of simulated wastewater was 7.5. Influent flowed through the column with an empty bed contact time (EBCT) of 10 or 20 min. The effluent samples were collected at regular intervals, filtered by a 0.45 μm membrane filter and then the phosphorus concentration was determined.

2.6. Analytical methods

Phosphorus (P) concentration was determined using an inductively coupled plasma atomic emission spectroscopy (ICP-AES, Optima 7100 DV, PerkinElmer Co., USA). Fe and Cu concentrations in the effluent were determined using an inductively coupled plasma mass spectrometer (ICP-MS, ELAN DRC II, PerkinElmer Co., USA). Prior to analysis, the aqueous samples were acidified with dilute HCl solution (1%), and stored in acid-washed plastic vessels. All samples were analyzed within 24 h after collection.

3. Results and discussion

3.1. Adsorption isotherms

To evaluate the maximal adsorption capacity of phosphate on the granular Fe-Cu binary oxide adsorbent, batch isotherm experiments have been performed at different pHs and temperatures. Fig. 1(a) illustrates the plots of adsorbed phosphate as a function of phosphate concentration in solution. It shows that GFC is more effective in adsorbing phosphate at pH 5.5 than that at pH 7.0, which is in agreement with the results from powered Fe-Cu binary oxide adsorbent [23]. Adsorption data were fitted with the Langmuir (Eq. (1)), Freundlich (Eq. (2)), and Temkin (Eq. (3)) models, which are extensively used to describe equilibrium adsorption data [29]. The Langmuir adsorption model is based on the assumptions that adsorption is limited to one monolayer, all surface sites are identical, and adsorption to one site is independent of the occupancy condition of the adjacent sites. The Freundlich model assumes that adsorption occurs on a heterogeneous surface and is multi-layer sorption. The Temkin model considers the effects of some indirect adsorbate/adsorbate interactions on adsorption and assumes that the heat of adsorption decreases linearly with respect to coverage, due to these interactions [29].

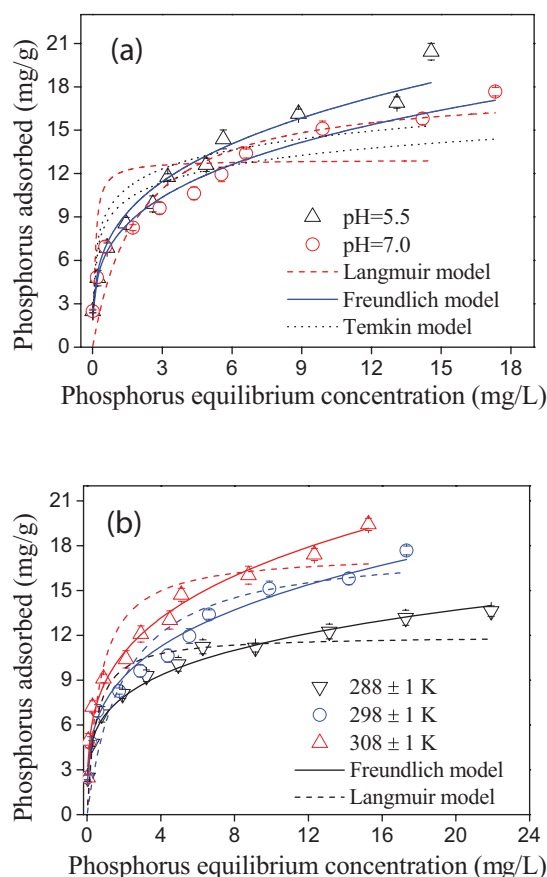


Fig. 1. Adsorption isotherm of phosphate on GFC at (a) two pH levels and (b) different temperatures.

$$q_e = \frac{q_{\max} K_L C_e}{1 + K_L C_e} \quad (1)$$

$$q_e = K_F C_e^{1/n} \quad (2)$$

$$q_e = \left(\frac{RT}{b} \right) \ln(AC_e) \quad (3)$$

where q_e and q_{\max} represent the amount of equilibrium adsorption capacity and the maximum adsorption capacity (mg/g), respectively; C_e is the equilibrium solution concentration (mg/L); K_L (L/mg) is the Langmuir coefficient; K_F is roughly an indicator of the adsorption capacity; n is the heterogeneity factor which has a lower value for more homogeneous surfaces; A (L/g) is the Temkin isotherm constant and b (kJ mol⁻¹) is the Temkin constant related to the heat of adsorption; R (8.314 J mol⁻¹ K⁻¹) is the universal gas constant, and T is the absolute temperature in kelvin.

The coefficient of determination (R^2) values in Table 1 suggest that the Freundlich model is the most suitable one for describing adsorption data at both pH levels. This is different from the model fitting results of powdered Fe-Cu binary oxide, where the Langmuir model is more suitable than Freundlich model for fitting the isotherm data [23]. This apparent discrepancy might be attributed to the introduction of PVA,

making the surface of GFC much more heterogeneous. The maximal adsorption capacity of GFC, calculated from Langmuir model, is 20.2 mg/g at pH 5.5 ± 0.1 and 17.2 mg/g at pH 7.0 ± 0.1 (Table 2). The value is greater than those of many other adsorbents, suggesting GFC is superior to them. Although granulation reduced the phosphate adsorption capacity of Fe-Cu binary oxide, GFC still retained over 50% of the maximal sorption capacity of powder Fe-Cu binary oxide.

Fig. 1(b) shows the influence of temperature on phosphate adsorption at pH 7.0 ± 0.1. The thermodynamic equilibrium constants (K_0) for the adsorption process was determined by plotting $\ln(q_e/C_e)$ vs. q_e and extrapolating q_e to zero using a graphical method. The change in Gibbs free energy (ΔG^0) was calculated using Eq. (4). The change in enthalpy (ΔH^0) and entropy (ΔS^0) was calculated from the slope and intercept of the plot of $\ln K_0$ vs. $1/T$ (Eq. (5)).

$$\Delta G^0 = -RT \ln K_0 \quad (4)$$

$$\ln K_0 = \frac{\Delta S^0}{R} - \frac{\Delta H^0}{RT} \quad (5)$$

where R is the universal gas constant (8.314 J mol⁻¹ K⁻¹), and T is the absolute temperature in kelvin.

Table 1

Langmuir, Freundlich, and Temkin isotherms parameters for phosphate adsorption on the GFC at two pH levels

pH	Langmuir model			Freundlich model			Temkin model		
	q_{\max} (mg·g ⁻¹)	k_L (L·mg ⁻¹)	R^2	k_F	$1/n$	R^2	A (mg L ⁻¹)	b (kJ mol ⁻¹)	R^2
5.5 ± 0.1	20.2	0.49	0.886	7.73	0.34	0.978	52.9	1.01	0.837
7.0 ± 0.1	17.2	0.60	0.836	7.43	0.29	0.985	90.1	1.21	0.863

Table 2

A comparison of maximum phosphate adsorption capacity (from Langmuir model) for different adsorbents

Adsorbent	Adsorbent state	Best model for fitting	P equilibrium concentration range (mg/L)	Solution pH	Maximum capacity (mg/g)	Reference
Fe-Cu binary oxide	Powder	Langmuir	0–25	5.0	39.8	[23]
Magnetic Fe-Zr oxide	Powder	Langmuir	0–100	4.0	13.6	[30]
Magnetic iron oxide	Powder	Freundlich	0–25	–	5.0	[31]
La-doped vesuvianite	Powder	Langmuir	0–4	7.1	6.7	[32]
Peat	Powder	Langmuir	0–120	5.2	8.9	[33]
Biochar	Powder	Freundlich	0–40	–	15.1	[15]
GAC	Granules	Langmuir	0–20	6.8	3.0	[34]
Chitosan modified zeolite	Granules	Langmuir	0–2	–	4.1	[35]
PVA hydrogel bead	Beads	Langmuir	0–60	6.0	11.5	[36]
GFC	Granules	Freundlich	0–18	5.5	20.2	This study
GFC	Granules	Freundlich	0–18	7.0	17.2	This study

It was found that phosphate adsorption capacity increased with temperature from 288 to 308 K (Fig. 1(b)), while ΔG^0 declined from -3.92 to -4.21 kJ mol $^{-1}$ (Table 3). The negative values of ΔG^0 indicate that the adsorption process is spontaneous. The positive value of ΔH^0 (13.26 kJ mol $^{-1}$) indicates the endothermic nature of phosphate adsorption process. The positive value of ΔS^0 (59.65 J mol $^{-1}$ K $^{-1}$) implies an increase in the degree of freedom during adsorption process. These results are consistent with the reports of other researchers who investigated the thermodynamics of phosphate sorption on iron oxides [31].

3.2. Effect of pH on phosphate adsorption

Solution pH is an important parameter to influence not only the species of phosphate in water but also the surface charge of adsorbents, which in turn affects phosphate adsorption by the adsorbents. In water, phosphate can exist as H_3PO_4 , $H_2PO_4^-$, HPO_4^{2-} , or PO_4^{3-} , depending on the pH ($pK_1 = 2.15$, $pK_2 = 7.20$, and $pK_3 = 12.33$). With a point of zero charge (pzc) of 7.3 (Fig. 9), GFC adsorbed more phosphate on the acidic side of pzc. As pH increased, phosphate adsorption decreased (Fig. 2), which is typical for anion adsorption by metal oxides [37]. When the solution pH was below 7.2, $H_2PO_4^-$ was the main species and GFC was positively charged, which facilitated the adsorption of phosphate. As pH increased, phosphate adsorption decreased. But the reduction was not significant in pH 7.3–10.0, due to the formation of stable inner-sphere complex of phosphate with GFC via ligand exchange reaction [23]. Thus, GFC is an effective adsorbent for phosphate over a wide pH range.

3.3. Adsorption kinetics

Fig. 3(a) shows the effect of time on phosphate adsorption by GFC at pH 7.0 ± 0.1 . It can be seen that phosphate

Table 3
Thermodynamic parameters for phosphate adsorption on GFC

T (K)	K_0	ΔG^0 (kJ mol $^{-1}$)	ΔS^0 (J mol $^{-1}$ K $^{-1}$)	ΔH^0 (kJ mol $^{-1}$)
288	5.14	-3.92	59.65	13.26
298	4.92	-3.95		
308	5.16	-4.21		

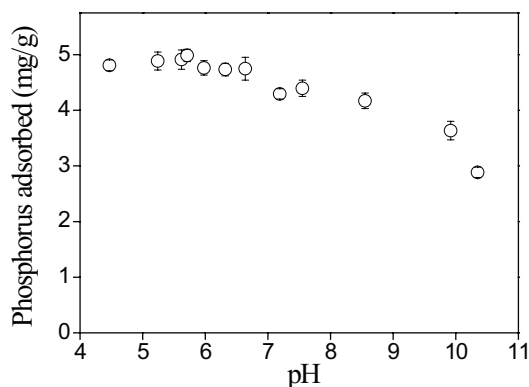


Fig. 2. Effect of solution pH on phosphate sorption on GFC.

adsorption was fast within the first 12 h and then slowed down. Adsorption equilibrium was reached at about 36 h, which was used in other batch adsorption tests. The kinetic data were initially fitted using the pseudo-first order (Eq. (6)), pseudo-second order (Eq. (7)), and Elovich (Eq. (8)) models as follows.

$$q_t = q_e(1 - e^{-k_1 t}) \tag{6}$$

$$q_t = \frac{q_e^2 k_2 t}{1 + q_e k_2 t} \tag{7}$$

$$q_t = \frac{1}{\beta} \ln(\alpha\beta) + \frac{1}{\beta} \ln t \tag{8}$$

where q_e and q_t are the adsorption capacities (mg/g) of the adsorbent at equilibrium and at any time, t (h), respectively; k_1 (h $^{-1}$) and k_2 (g mg $^{-1}$ h $^{-1}$) are the pseudo-first order and pseudo-second order rate constants for adsorption process, respectively; α is the initial adsorption rate constant and β is the Elovich adsorption constant. The fitting results are shown in Fig. 3(a) and the related values of parameters are summarized in Table 4. The high R^2 values suggest that both the pseudo-first order model and pseudo-second order model

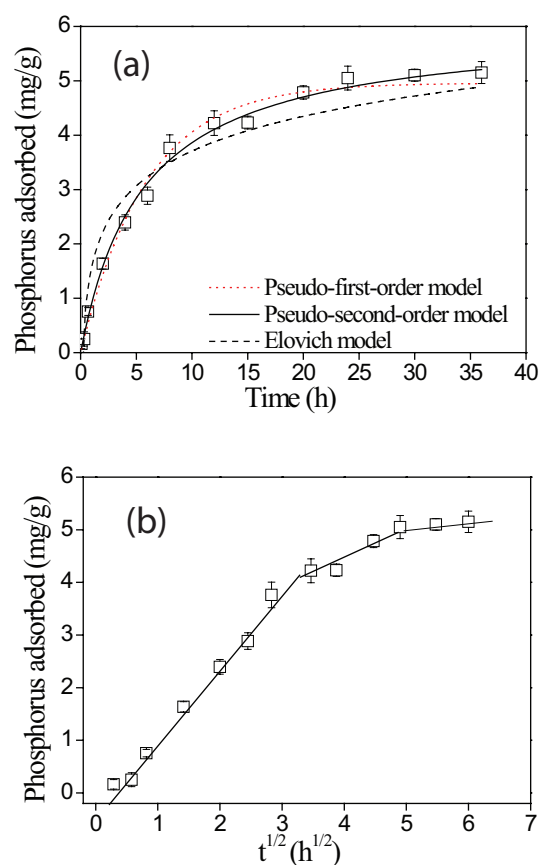


Fig. 3. Kinetics of phosphate adsorption on GFC at pH 7.0 ± 0.1 . (a) Fitted with pseudo-first order, pseudo-second order, and Elovich models and (b) fitted with intraparticle diffusion model.

Table 4
Kinetic parameters for phosphate adsorption on GFC fitted with different models

pH	Pseudo-first order			Pseudo-second order			Elovich		
	q_e (mg·g ⁻¹)	k_1 (h ⁻¹)	R^2	q_e (mg·g ⁻¹)	K_2 (g·mg ⁻¹ ·h ⁻¹)	R^2	α (mg·g ⁻¹ ·h ⁻¹)	β (g·mg ⁻¹)	R^2
7.0	5.1	0.16	0.991	6.1	5.77	0.995	4.99	1.03	0.937

fitted the kinetic data well. Elovich model was less suitable for describing phosphate adsorption kinetic process. These results indicated that both physical and chemical adsorption might be involved in the adsorption process.

Adsorption is a multi-step process and involves four sequential steps: diffusion through the bulk liquid, film diffusion, intraparticle diffusion, and adsorption on the solid surface [38]. Because the pseudo-second order model takes adsorption as a single, one-step binding process [39], its accuracy would be affected when applied to granular adsorbents. Intraparticle diffusion model is extensively used for describing adsorbate sorption by granular adsorbents because it considers adsorption as a process containing a series of distinct steps [39]. Therefore, the kinetic data were also fitted using the intraparticle diffusion model (Eq. (9)) and the result is shown in Fig. 3(b).

$$q_t = k_p t^{0.5} + c \quad (9)$$

where q_t is the amount of adsorbed phosphorus at any time t (h), k_p is the intraparticle diffusion rate constant, and the constant C (mg/g) represents the boundary layer effect. k_p and C can be determined from the plot of q_t vs. $t^{0.5}$. If intraparticle diffusion is the rate-controlling step, the plot of q_t against $t^{0.5}$ should be linear and pass through the origin [24]. Fig. 3(b) shows three linear sections, implying three stages in adsorption processes: fast, moderate, and slow. They might be dominated by external mass transfer, intraparticle diffusion and steric hindrance from the adsorbed phosphate molecules, respectively. This suggests that the phosphate sorption on GFC is a multi-step process and intraparticle diffusion is not the rate-controlling step. Obviously, intraparticle diffusion model is much more suitable for describing the sorption process of phosphate on the GFC.

3.4. Effect of coexisting anions

Anions such as SO_4^{2-} , HCO_3^- , and SiO_3^{2-} often exist in natural waters. They might compete with phosphate for sorptive sites on the surface of an adsorbent and hinder phosphate adsorption. Fig. 4 indicates that the coexisting SO_4^{2-} , HCO_3^- , and SiO_3^{2-} had no significant effect on phosphate adsorption, even when their concentrations were almost one order of magnitude higher than that of phosphate. At much higher concentration levels (10 mM), these anions suppressed the phosphate adsorption by less than 20%. Thus, GFC is highly selective towards phosphate, and it has a good potential for use in real wastewater treatment. In addition, among three anions, SiO_3^{2-} caused the greatest decrease in phosphate adsorption. Silicon and phosphorus are located in the adjacent position in the periodic table of elements, and the molecular structure of the silicate ion is similar to

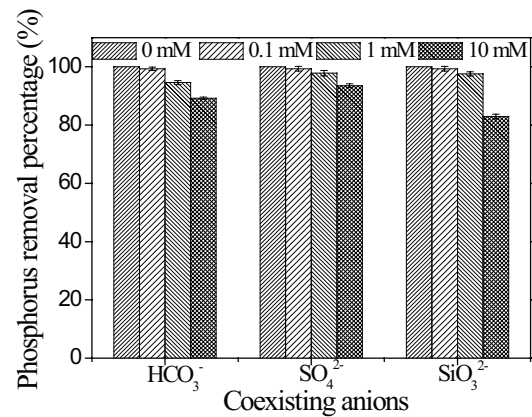


Fig. 4. Effect of coexisting anions on phosphate adsorption on GFC at pH 7.0 ± 0.1 .

that of the phosphate ion. Therefore, silicate could strongly compete with phosphate for available sorption sites on the surface of the GFC. Similar phenomenon was also observed by Konhauser et al. [40] when they studied the adsorption of phosphate on ferric oxyhydroxides.

3.5. Column tests

The GFC was packed in a fixed-bed column and the simulated wastewater was flowed through the column. The effluent histories of phosphate are demonstrated in Fig. 5. The phosphate concentration in influent is 3.2 mg/L and solution pH is 7.2. When the EBCT was 10 min, more than 900 bed volumes of simulated phosphorus-containing wastewater were treated before the phosphate concentration in the effluent reached the limit of 50 $\mu\text{g/L}$. For a longer EBCT of 20 min, about 1,780 bed volumes of simulated wastewater were treated before the breakthrough. Apparently, a longer EBCT favors the diffusion of phosphate in the pores and more complete utilization of surface sorptive sites of the GFC. Above-mentioned results suggest that the GFC is an effective phosphorus adsorbent and can be used in real wastewater treatment. In addition, the release of Fe and Cu from the GFC was investigated, to evaluate the possibility of secondary pollution during the process of GFC utilization in column tests. It was found that the Fe and Cu concentrations in the effluent were both less than 0.05 mg/L, which met the limits of drinking water. Therefore, GFC was stable and safe to use, with little risk of secondary pollution during water treatment.

3.6. Characterization of GFC before and after phosphate adsorption

The as-prepared GFC is cylindrical, with a diameter of approximate 2.0 mm and a length of 2.0–3.0 mm (Fig. 6).

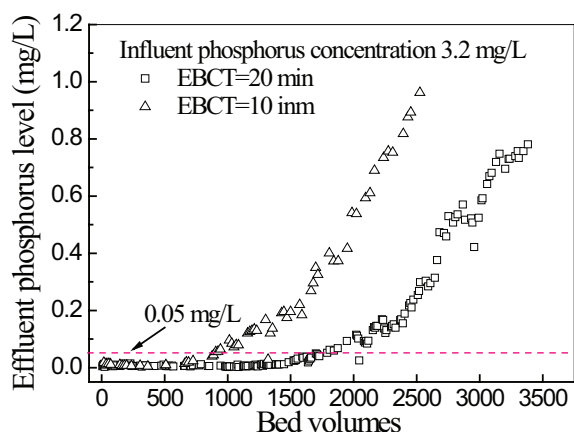


Fig. 5. Breakthrough curves for phosphate adsorption by GFC from the simulated wastewater.



Fig. 6. Photograph of granular Fe-Cu binary oxide sorbent.

Fig. 7 shows the field emission scanning electron microscope (FE-SEM) images of the GFC with different magnification. It can be seen that the GFC is aggregate of nanoparticles and its surface is relatively rough. X-ray diffraction pattern of the GFC is illustrated in Fig. 8(a). It demonstrates two broad peaks at approximately 35.3° and 62.1° , which are very similar to those of pure Fe-Cu binary oxide and poorly ordered 2-line ferrihydrite [41]. In addition, the sharp peak appearing at 16.2° might be ascribed to the PVA component. The FTIR spectrum of the GFC is shown in Fig. 8(b). The broad peak at $3,200\text{--}3,600\text{ cm}^{-1}$ is attributed to the stretching vibration of -OH ; the peaks at $2,924\text{ cm}^{-1}$ is assigned to the asymmetric stretching vibration of -CH_2 ; the peak at $2,854\text{ cm}^{-1}$ is assigned to the symmetric stretching vibration of -CH_2 ; the peak at $1,632\text{ cm}^{-1}$ is assigned to the deformation of water molecules, which indicates the presence of physisorbed water; the peaks at $1,431\text{ cm}^{-1}$ is assigned to the bending vibration of CH-OH ; the peak at $1,107\text{ cm}^{-1}$ is attributed to the vibration of SO_4^{2-} [42]; the peak at 675 cm^{-1} may be assigned to the bending vibration of C-H . GFC had a BET specific surface area of $62\text{ m}^2/\text{g}$, much lower than that of the original powdered Fe-Cu binary oxide ($282\text{ m}^2/\text{g}$) [41]. Obviously, granulation reduced the specific surface area of

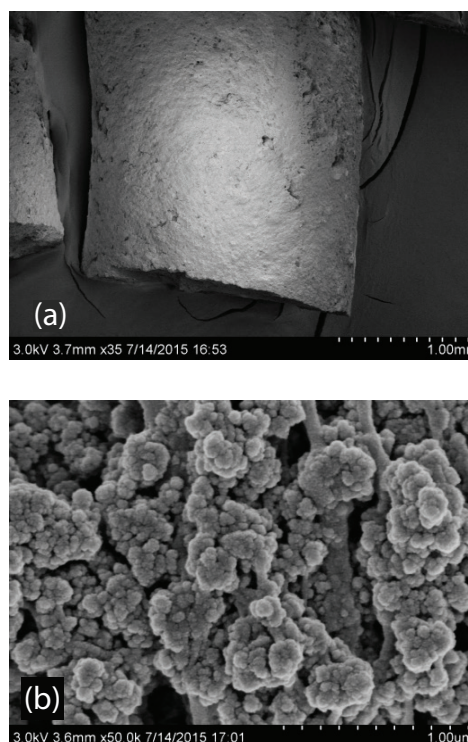


Fig. 7. FE-SEM images of the granular Fe-Cu binary oxide, (a) ($\times 35$) and (b) ($\times 50,000$).

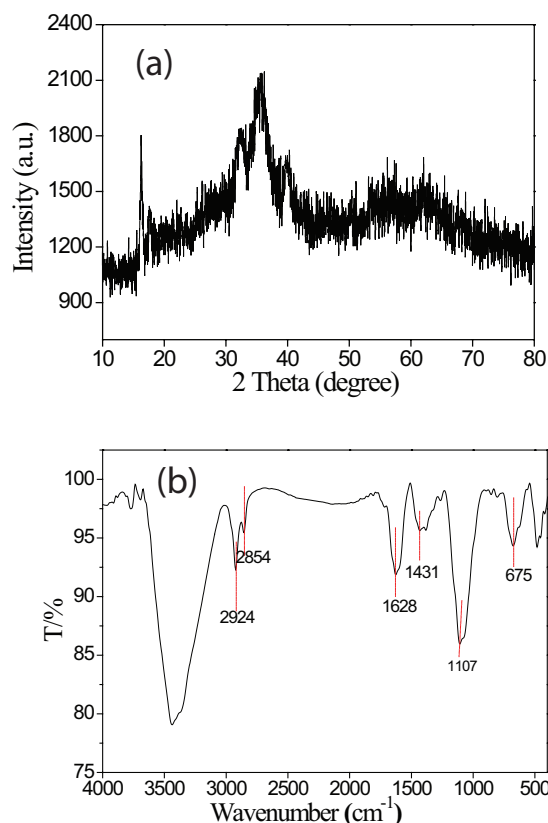


Fig. 8. (a) XRD diffraction pattern and (b) FTIR spectrum of the GFC.

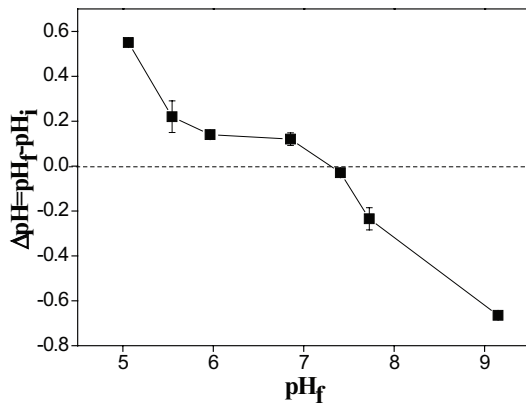


Fig. 9. Point of zero charge (pzc) determination for GFC. ΔpH is the change in pH during 3 h after increasing the electrolyte concentration, and pzc is the pH at which $\Delta\text{pH} = 0$.

Fe-Cu binary oxide by 78%. This contributes to the decrease in phosphate maximal adsorption capacity though to a less extent (less than 50%). The point of zero charge (pzc) of GFC is found to be 7.3 (Fig. 9). It is slightly lower than that of Fe-Cu binary oxide (7.9) but very close to that of pure ferrihydrite (7.4) [41]. This decrease in pzc might be ascribed to the introduction of PVA.

The elemental distributions of Fe, Cu, and P on the cross section of GFC before and after phosphate adsorption are shown in Fig. 10. Before phosphate adsorption, the Fe and Cu were uniformly distributed on the cross section. After P adsorption, the distribution of Fe and Cu did not significantly change, while the distribution of adsorbed phosphate showed different characteristics. Most of the adsorbed phosphate was located on the edge of GFC particles, whereas P concentration in the center of particles was minimum. This was expected because phosphate first diffused across the edge of GFC particles, then gradually penetrated into

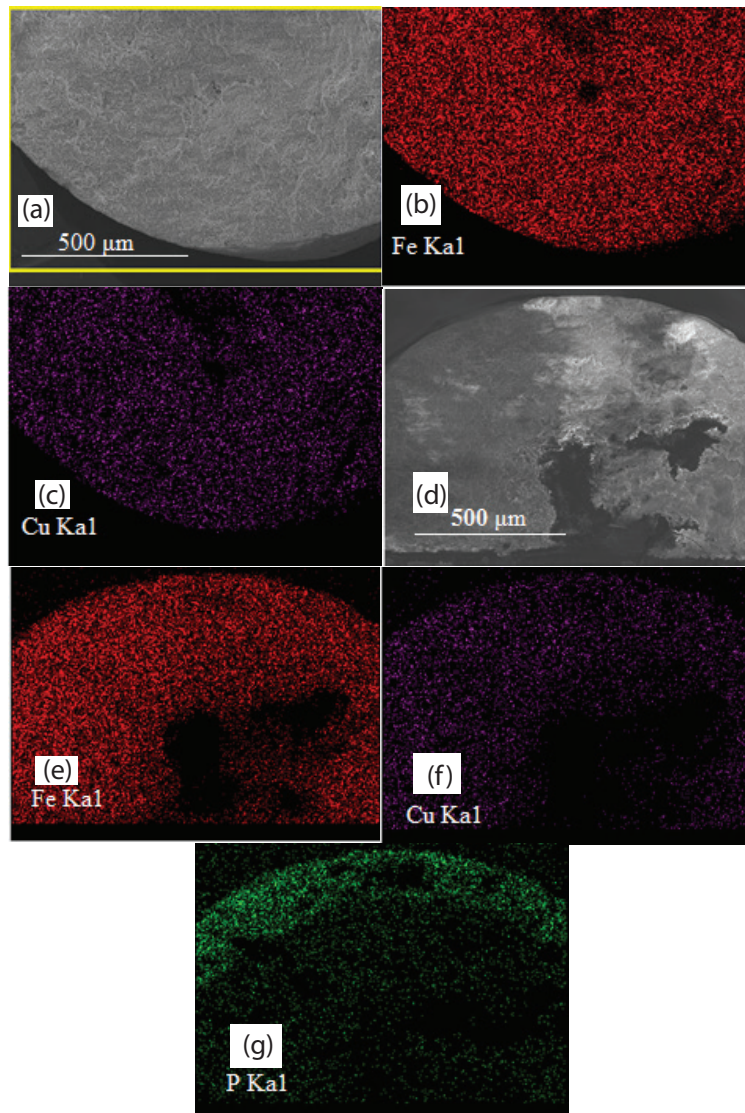
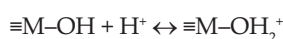


Fig. 10. FE-SEM images and elemental maps of cross section of GFC. Image (a), Fe-K (b), and Cu-K (c) for original GFC; image (d), Fe-K (e), Cu-K (f), and P-K (g) for P adsorbed GFC.

interior part and finally reached the center during phosphate adsorption.

Under neutral condition, a possible mechanism for phosphate removal by the GFC can be proposed, which is similar to that of pure Fe-Cu binary oxide. Phosphate ions are removed through the replacement of surface hydroxyl groups on the Fe-Cu binary oxide surface and formation of monodentate mononuclear and/or bidentate binuclear inner-sphere surface complexes. The possible reactions between phosphate ions and the surface of GFC could be presented as follows:



monodentate mononuclear



bidentate binuclear

where -OH is a hydroxyl group.

4. Conclusions

A novel GFC adsorbent was prepared with extrusion granulation method. It has good mechanical property and adsorption performance towards phosphate. The maximal adsorption capacity for phosphorus is 20.2 mg/g at pH 5.0 ± 0.1 , which is superior to most of reported granular sorbents. The phosphate adsorption increased with increasing temperature, but decreased with an increase in solution pH. The co-existing SO_4^{2-} , HCO_3^- , and SiO_3^{2-} had no significant effect on phosphate adsorption. The GFC could be readily applied to a fixed-bed system for phosphate removal and about 1,780 bed volumes of simulated phosphorus-containing wastewater were treated before the phosphorus concentration in the effluent reached 0.05 mg/L for an EBCT of 20 min. The GFC has high potential to be used for phosphate removal in real wastewater treatment, due to its high performance and selectivity.

Acknowledgements

This work was financially supported by the National Natural Science Foundation of China (Grant No. 51478457) and the open Fund of the Jiangsu Key Laboratory for Environment Functional Materials (No. SJHG1312).

References

- [1] J. Das, B.S. Patra, N. Baliarsingh, K.M. Parida, Adsorption of phosphate by layered double hydroxides in aqueous solutions, *Appl. Clay Sci.*, 32 (2006) 252–260.
- [2] S.M. Ashekuzzaman, J.Q. Jiang, Study on the sorption-desorption-regeneration performance of Ca-, Mg- and CaMg-based layered double hydroxides for removing phosphate from water, *Chem. Eng. J.*, 246 (2014) 97–105.
- [3] X. Xu, B.Y. Gao, Q.Y. Yue, Q.Q. Zhong, Sorption of phosphate onto giant reed based adsorbent: FTIR, Raman spectrum analysis and dynamic sorption/desorption properties in filter bed, *Bioresour. Technol.*, 102 (2011) 5278–5282.
- [4] U.S. Environmental Protection Agency (USEPA), Quality Criteria for Water, Office of Water, Regulation and Standard, Washington, D.C. 20460, EPA 440/5-86-001, 1986.
- [5] Florida Everglades Forever Act, Florida State Legislature, Tallahassee, Florida, 1994.
- [6] L.M. Blaney, S. Cinar, A.K. SenGupta, Hybrid anion exchanger for trace phosphate removal from water and wastewater, *Water Res.*, 41 (2007) 1603–1613.
- [7] A. Soares, M. Veeram, F. Simoes, E. Wood, S.A. Parsons, T. Stephenson, Bio-struvite: a new route to recover phosphorus from wastewater, *Clean Soil Air Water*, 42 (2014) 994–997.
- [8] E.M.v. Voorthuizen, A. Zwijnenburg, M. Wessling, Nutrient removal by NF and RO membranes in a decentralized sanitation system, *Water Res.*, 39 (2005) 3657–3667.
- [9] A. Oehmen, P.C. Lemos, G. Carvalho, Z. Yuan, J. Keller, L.L. Blackall, M.A. Reis, Advances in enhanced biological phosphorus removal: from micro to macro scale, *Water Res.*, 41 (2007) 2271–2300.
- [10] X.X. Ju, S.B. Wu, Y.S. Zhang, R.J. Dong, Intensified nitrogen and phosphorus removal in a novel electrolysis-integrated tidal flow constructed wetland system, *Water Res.*, 59 (2014) 37–45.
- [11] L. De-Bashan, Y. Bashan, Recent advances in removing phosphorus from wastewater and its future use as fertilizer (1997–2003), *Water Res.*, 38 (2004) 4222–4246.
- [12] R. Chitrakar, S. Tezuka, A. Sonoda, K. Sakane, K. Ooi, T. Hirotsu, Phosphate adsorption on synthetic goethite and akaganeite, *J. Colloid Interface Sci.*, 298 (2006) 602–608.
- [13] L. Bouhouf, C. Boukhalfa, L. Reinert, L. Duclaux, Characterization of phosphate removal from aqueous solution by manganese oxyhydroxide, *Desal. Wat. Treat.*, 89 (2017) 274–279.
- [14] W. Chen, L. Li, W. Zhang, F. Xu, M. Niu, J. Wang, Y. Wang, Microwave-assisted dried volcanic tephra/calcium alginate composite for phosphate removal from micro-polluted wastewater, *Clean Soil Air Water*, 42 (2014) 561–570.
- [15] F. Peng, P.-W. He, Y. Luo, X. Lu, Y. Liang, J. Fu, Adsorption of phosphate by biomass char deriving from fast pyrolysis of biomass waste, *Clean Soil Air Water*, 40 (2012) 493–498.
- [16] R. Chintala, T.E. Schumacher, L.M. McDonald, D.E. Clay, D.D. Malo, S.K. Papiernik, S.A. Clay, J.L. Julson, Phosphorus sorption and availability from biochars and soil/biochar mixtures, *Clean Soil Air Water*, 42 (2014) 626–634.
- [17] O.R. Harvey, R.D. Rhue, Kinetics and energetics of phosphate sorption in a multi-component Al(III)–Fe(III) hydr(oxide) sorbent system, *J. Colloid Interface Sci.*, 322 (2008) 384–393.
- [18] Y. Su, W.Y. Yang, W.Z. Sun, Q. Li, J.K. Shang, Synthesis of mesoporous cerium–zirconium binary oxide nanoadsorbents by a solvothermal process and their effective adsorption of phosphate from water, *Chem. Eng. J.*, 268 (2015) 270–279.
- [19] G.S. Zhang, H.J. Liu, R.P. Liu, J.H. Qu, Removal of phosphate from water by a Fe–Mn binary oxide adsorbent, *J. Colloid Interface Sci.*, 335 (2009) 168–174.
- [20] Z.M. Ren, L.N. Shao, G.S. Zhang, Adsorption of phosphate from aqueous solution using an iron–zirconium binary oxide sorbent, *Water Air Soil Pollut.*, 223 (2012) 4221–4231.
- [21] J.B. Lü, H.J. Liu, R.P. Liu, X. Zhao, L.P. Sun, J.H. Qu, Adsorptive removal of phosphate by a nanostructured Fe–Al–Mn trimetal oxide adsorbent, *Powder Technol.*, 233 (2013) 146–154.
- [22] W. Zhang, X.W. Wang, J. Chen, G.S. Zhang, Highly efficient removal of phosphate using a novel Fe–La binary (hydro) oxide as adsorbent: behavior and mechanism, *Desal. Wat. Treat.*, 83 (2017) 98–110.
- [23] G.L. Li, S. Gao, G.S. Zhang, X.W. Zhang, Enhanced adsorption of phosphate from aqueous solution by nanostructured iron(III)-copper(II) binary oxides, *Chem. Eng. J.*, 235 (2014) 124–131.
- [24] X.M. Dou, Y.S. Zhang, H.J. Wang, T.J. Wang, Y.L. Wang, Performance of granular zirconium-iron oxide in the removal of fluoride from drinking water, *Water Res.*, 45 (2011) 3571–3578.
- [25] L.L. Ma, N. Chen, C.P. Feng, Comparison of phosphorus removal characteristics using synthesized Fe-loaded granular composites, *Desal. Wat. Treat.*, 77 (2017) 221–228.
- [26] C. Vervaet, J.P. Remon, Continuous granulation in the pharmaceutical industry, *Chem. Eng. Sci.*, 60 (2005) 3949–3957.

- [27] E. Ahmadi, M.N. Haghghi, Z. Mohamadnia, A. Ramazani, Preparation of shishkebab and nanofiber polyethylene with chromium/santa barbara amorphous silica-15 catalysts, *J. Appl. Polym. Sci.*, 118 (2010) 3658–3665.
- [28] D.G. Kinniburgh, J.K. Syers, M.L. Jackson, Specific adsorption of trace amounts of calcium and strontium by hydrous oxides of iron and aluminum, *Soil Sci. Soc. Am. Proc.*, 39 (1975) 464–470.
- [29] J. Lalley, C. Han, X. Li, D.D. Dionysiou, M.N. Nadagouda, Phosphate adsorption using modified iron oxide-based sorbents in lake water: kinetics, equilibrium, and column tests, *Chem. Eng. J.*, 284 (2016) 1396–1396.
- [30] F. Long, J.L. Gong, G.M. Zeng, L. Chen, X.Y. Wang, J.H. Deng, Q.Y. Niu, H.Y. Zhang, X.R. Zhang, Removal of phosphate from aqueous solution by magnetic Fe-Zr binary oxide, *Chem. Eng. J.*, 171 (2011) 448–455.
- [31] S.Y. Yoon, C.G. Lee, J.A. Park, J.H. Kim, S.B. Kim, S.H. Lee, J.W. Choi, Kinetic, equilibrium and thermodynamic studies for phosphate adsorption to magnetic iron oxide nanoparticles, *Chem. Eng. J.*, 236 (2014) 341–347.
- [32] H. Li, J.Y. Ru, W. Yin, X.H. Liu, J.Q. Wang, W.D. Zhang, Removal of phosphate from polluted water by lanthanum doped vesuvianite, *J. Hazard. Mater.*, 168 (2009) 326–330.
- [33] J.B. Xiong, Q. Mahmood, Adsorptive removal of phosphate from aqueous media by peat, *Desalination*, 259 (2010) 59–64.
- [34] S. Hussain, H.A. Aziz, M.H. Isa, A. Ahmad, J.V. Leeuwen, L. Zou, S. Beecham, M. Umar, Orthophosphate removal from domestic wastewater using limestone and granular activated carbon, *Desalination*, 271 (2011) 265–272.
- [35] J. Xie, C. Li, L. Chi, D. Wu, Chitosan modified zeolite as a versatile adsorbent for the removal of different pollutants from water, *Fuel*, 103 (2013) 480–485.
- [36] B. Hui, Y. Zhang, L. Ye, Preparation of PVA hydrogel beads and adsorption mechanism for advanced phosphate removal, *Chem. Eng. J.*, 235 (2014) 207–214.
- [37] W. Stumm, *Chemistry of the Solid–Water Interface*, Wiley Interscience, New York, 1996.
- [38] M. Badruzzaman, P. Westerhoff, D.R.U. Knappe, Intraparticle diffusion and adsorption of arsenate onto granular ferric hydroxide (GFH), *Water Res.*, 38 (2004) 4002–4012.
- [39] M. D’Arcy, D. Weiss, M. Bluck, R. Vilar, Adsorption kinetics, capacity and mechanism of arsenate and phosphate on a bifunctional TiO₂-Fe₂O₃ bi-composite, *J. Colloid Interface Sci.*, 364 (2011) 205–212.
- [40] K.O. Konhauser, S.V. Lalonde, L. Amskold, H.D. Holland, Was there really an Archean phosphate crisis?, *Science*, 315 (2007) 1234–1234.
- [41] G.S. Zhang, Z.M. Ren, X.W. Zhang, J. Chen, Nanostructured iron(III)-copper(II) binary oxide: a novel adsorbent for enhanced arsenic removal from aqueous solutions, *Water Res.*, 47 (2013) 4022–4031.
- [42] G. Lefevre, In situ Fourier-transform infrared spectroscopy studies of inorganic ions adsorption on metal oxides and hydroxides, *Adv. Colloid Interface*, 107 (2004) 109–123.